AJNR

MR-gated intracranial CSF dynamics: evaluation of CSF pulsatile flow.

P C Njemanze and O J Beck

AJNR Am J Neuroradiol 1989, 10 (1) 77-80
http://www.ajnr.org/content/10/1/77

MR-Gated Intracranial CSF Dynamics: Evaluation of CSF Pulsatile Flow

Philip Chidi Njemanze[1,2]
Oscar Josef Beck

This article describes a new imaging method, called MR-gated intracranial CSF (liquor) dynamics, or MR-GILD. Pulsatile flow in CSF pathways is revealed by the difference between diastolic- and systolic-gated images. The images clearly demonstrate the ventricles, cisterns, and vascular structures. The dependence of CSF movement on arterial pulse transformation is analyzed, illustrative cases are given to show some pathologic variations, and the use of MR-GILD for neurosurgical patients is discussed.

MR imaging has been used to evaluate flow effects, not only in vascular structures [1–4] but also in the CSF flow pathway [5, 6]. A CSF flow-void sign has been identified in the foramina of Monro, aqueduct of Sylvius, and foramen of Magendie. Its occurrence has been related to the cardiac cycle. This effect is caused by spin-phase shifts and time-of-flight effects created as a result of CSF turbulence and increased velocity of CSF pulsatile flow [6].

The purpose of this study is to describe the use of the MR-gated intracranial CSF (liquor) dynamics, or MR-GILD, technique—which is based on a bipolar gradient pulse sequence—to demonstrate CSF pulsatile flow in ventricles and cisterns as a means of analyzing CSF circulatory system dynamics in neurosurgical patients.

Subjects and Methods

Eleven patients with CSF circulatory disease and three normal subjects were examined. Multislice MR imaging studies were obtained by using a Siemens MR imaging system operating at 1.0 T. Data were acquired with a 256 × 256 matrix and two-dimensional Fourier transformation. Scans were reconstructed and interpolated into a 512 × 512 image matrix. Each patient was positioned comfortably in the standard Siemens saddle head coil. Slice thickness was 5 mm, and three slices were acquired. An echo time (TE) of 50 msec was used. RF stimulation and all scan data acquisitions were grated to the QRS complex and therefore the repetition time (TR) was at least twice the patients' R-R interval and always between 1700–2000 msec.

An axial scout image was first acquired and the slice of interest was chosen, always in the midsaggital plane, although in some cases axial images were also acquired. A bipolar pulse consisting of two successive gradient pulses equal in magnitude and duration but of opposite sign was inserted into the pulse sequence between the 90° RF pulse and the readout gradient [7]. The first gradient pulse dephases the nuclei in the applied direction and the second pulse rephases them. Stationary nuclei were all brought back into phase, whereas for nuclei in motion along the gradient the rephasing was not complete, leaving them with a phase shift proportional to velocity. The phase difference (P_{diff}) due to motion, for a given velocity component, v, in the direction of the applied slice selection gradient, G, is $P_{diff} = -Y\ G\ v\ t_r\ t_{diff}$, where t_r is the duration of the rephasing pulse, t_{diff} is the difference in pulse separation for the two pulse sequences, and Y is the gyromagnetic ratio for protons.

The systolic time data acquisition (STDA) images were at 300 msec after the R wave, and the diastolic time data acquisition (DTDA) images were at 40 msec. Scan times were approximately 10 min. Two phase images were acquired, each with different velocity encod-

Received September 16, 1987; accepted after revision June 2, 1988.

Presented at the annual meeting of the American Roentgen Ray Society, San Francisco, May 1988.

This work was supported in part by the Catholic Service for Foreign Trainees (KAAD Bonn).

[1] Both authors: Department of Neurosurgery, Clinicum Grosshadern, Ludwig Maximillians-University, Munich, F.R.G.

[2] Present address: Non Invasive Flow Laboratory, P.O. Box 302, Owerri Imo State, Nigeria. Address reprint requests to P. C. Njemanze.

AJNR **10:77–80, January/February 1989**
0195-6108/89/1001-0077

ing, which was achieved by varying the temporal separation of the dephase and rephase components of the slice selection gradient. The final flow image was obtained by subtracting these two images at systolic and diastolic times for the same slice position. The order of subtraction was important for the flow intensities seen on the subtraction images. When the rephasing images were placed first, subtraction yielded images of higher intensities, especially in the respiratory pathways and surrounding air movement. On the other hand, for pulsatile motion, flow effects are caused by spins moving at different velocities along a magnetic field gradient. In bulk flow, these effects include signal enhancement by replacement of partially saturated spins by unexcited upstream spins and signal attenuation due to loss of 90° excited spins from the 180° refocusing region.

Results

In all subjects it was possible to demonstrate the CSF and vascular pulsatile flow. Four illustrative cases are presented to describe the MR-GILD technique. Similar flow effects to these were seen in the other subjects.

Case 1

A 29-year-old woman had mild symptoms of raised intracranial pressure. CT showed moderately enlarged ventricles, and aqueductal stenosis was suspected. The MR-GILD technique images, DTDA (Fig. 1A) and STDA (Fig. 1B), showed irregular contours of the aqueduct of Sylvius considerably narrowing the lumen at two points, more pronounced in diastole than in systole. It seemed that the aqueduct was almost closed in diastole and then opened in systole. A valve mechanism of CSF drainage was proposed. Since the diastolic time is longer than the systolic time, this could lead to accumulation of excess CSF in the lateral ventricles, explaining the symptoms of hydrocephalus. The height of the third ventricle appeared greater in diastole than in systole. At the foramen of Monro, CSF pulsatile flow was demonstrated with more flow signal in systole. No significant change of signal in the basal cisterns was seen. In the nasal fossa, signal enhancement was caused by the replacement of partially saturated spins by unexcited spins at the different phases of the respiratory cycle; in the subtracted image there is a high-intensity signal yield. A similar effect is seen in Fig. 3D, the difference being that the rephasing image was placed first in the subtraction procedure.

Case 2

A 41-year-old man with Crouzon disease, an autosomal dominant inherited trait, had several abnormalities of the skull [8]. The clivus was oriented more vertically than usual and the sphenoid plane was angled downward and forward. The floor of the frontal fossa was shorter than normal in the anteroposterior direction, while the transverse diameter of the skull was enlarged. The patient had mild symptoms of increased intracranial pressure, with papilledema, visual loss, and exophthalmos. Cephalometry showed microcephaly. The MR-GILD images demonstrated the CSF pulsatile flow in the foramen of Monro, third ventricle, aqueduct of Sylvius, fourth ventricle, foramen of Magendie, cisterna magna, basal cisterns (interpeduncular cistern and cisterna pontis), and spinal subarachnoid space. There was a difference of diastolic and systolic images at the foramen of Monro, third ventricle, and fourth ventricle (Fig. 2).

Case 3

A 13-year-old boy had symptoms of raised intracranial pressure. Plain X-ray, CT (Fig. 3A), and T1-weighted MR imaging (Fig. 3B) showed the radiologic signs of raised intracranial pressure: suture diastasis, erosion of the dorsum sellae, increased convolutional markings, pineal displacement, wide ventricles, and periventricular hypodensity. The MR-GILD images showed minimal CSF flow signal in the foramina of Monro and no sign of flow in the third ventricle or aqueduct. CSF flow was observed in the cisterna pontis, the cervical spinal subarachnoid space, and the fourth ventricle (Fig. 3C).

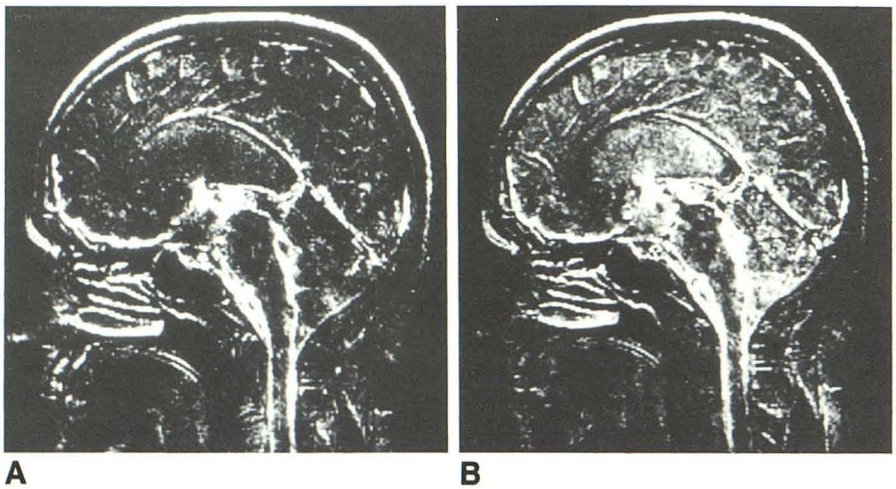

Fig. 1.—Case 1.
***A*, Diastolic time data acquisition (DTDA) image shows a larger third ventricle and narrower aqueduct of Sylvius as compared with the systolic time data acquisition (STDA) image (*B*).**
***B*, STDA image shows signal-rich foramen of Monro, foramen of Magendie, fourth ventricle, basal cisterns, cisterna magna, and spinal subarachnoid space, with a wider aqueduct of Sylvius.**

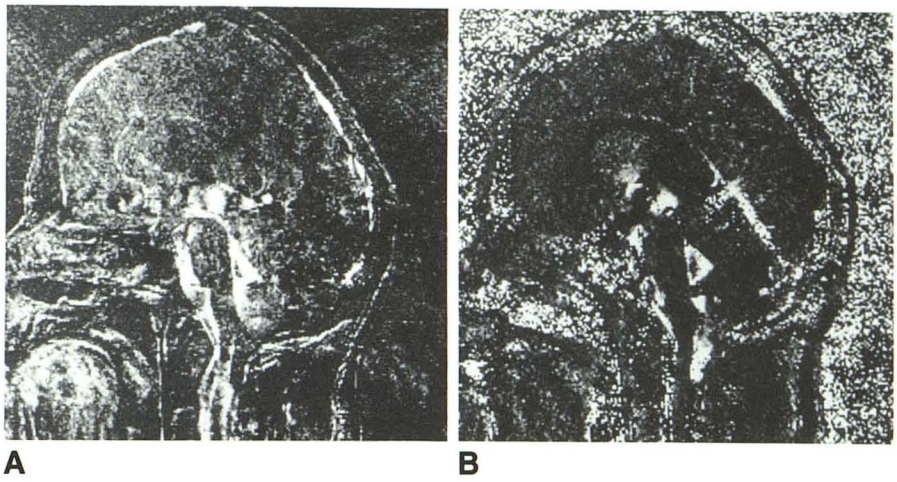

Fig. 2.—Case 2.
***A*, Diastolic time data acquisition (DTDA) image shows CSF pulsatile flow in the third ventricle, aqueduct of Sylvius, fourth ventricle, cisterna pontis, and interpeduncular cistern. Note abnormal configuration of the skull.**
***B*, Systolic time data acquisition (STDA) image shows CSF pulsatile flow in the foramen of Monro, third ventricle, fourth ventricle, foramen of Magendie, cisterna magna, cisterna pontis, and interpeduncular cistern.**

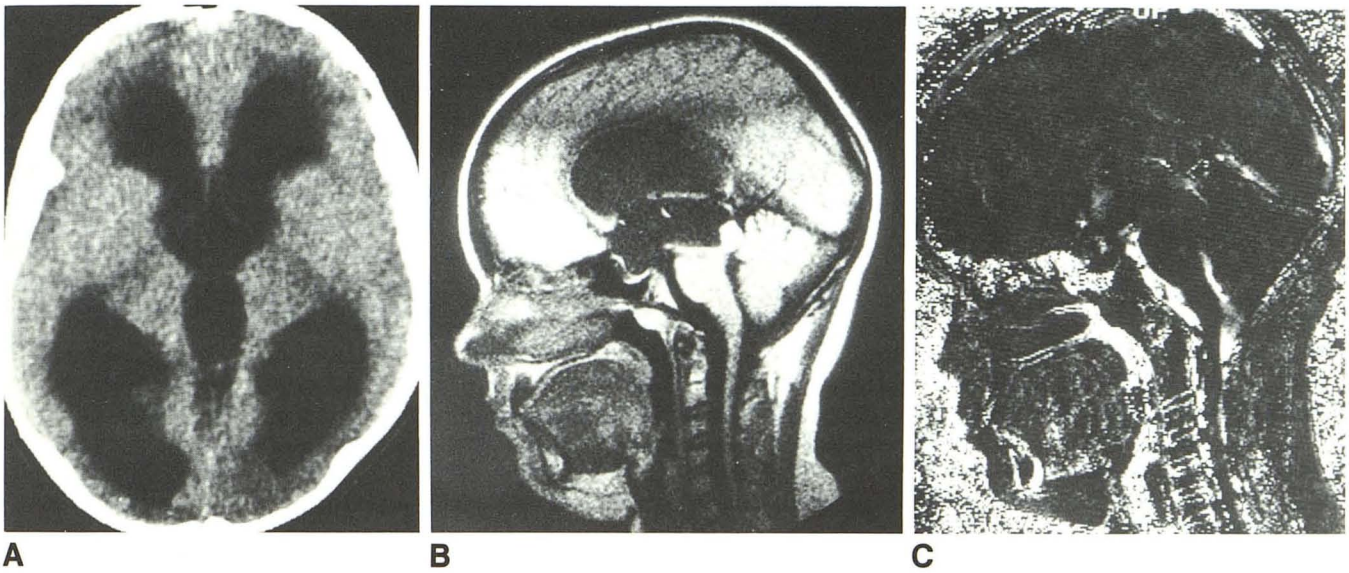

Fig. 3.—Case 3.
***A*, Axial CT scan shows wide lateral and third ventricles.**
***B*, T1-weighted sagittal MR image.**
***C*, Systolic time data acquisition (STDA) image shows CSF flow signal loss at foramen of Monro and third ventricle, but signal enhancement in the cisterna pontis, fourth ventricle, and spinal subarachnoid space.**

Case 4

An 11-year-old girl with symptoms of obstructive hydrocephalus, which had been observed in early childhood and managed with a ventriculoperitoneal shunt, was admitted to our clinic because of shunt dysfunction and symptoms of raised intracranial pressure. CT findings (Fig. 4A) revealed a very large fourth ventricle. MR-GILD (Fig. 4B) showed no CSF flow signs in the third ventricle, foramen of Monro, aqueduct of Sylvius, foramen of Magendie, cisterna magna, cisterna pontis, or spinal subarachnoid space. The pulsatile flow was well seen in the midline vascular structures: sigmoid sinus, sinus rectus, vein of Galen, internal cerebral vein, basilar artery, and pericallosal artery. The inferior occlusion at the level of the foramen of Magendie was demonstrated. An entrapped fourth ventricle was seen.

Discussion

O'Connell [9] suggested that the cardiac and respiratory pulses were the main source of CSF pulsation, but Bering [10] maintained that these pulsations had their origin in the pulsations of the chorioid plexuses. DuBoulay et al. [11] used X-ray cinematography and oil contrast medium to show that forceful CSF pulsation occurs in the spinal subarachnoid space, the cisterna magna, and the basal cisterns.

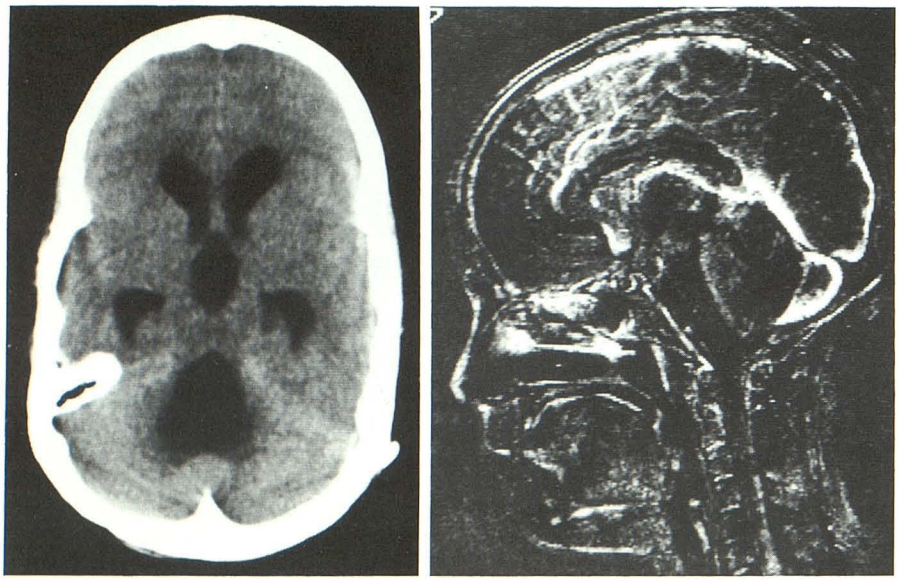

A B

Fig. 4.—Case 4.
***A*, Axial CT scan shows wide IV ventricle.**
***B*, Systolic time data acquisition (STDA) image (see text for discussion).**

A pump action—referred to as "third ventricular, or thalamic, pump" that consisted largely of a rhythmic squeeze between the two thalami, which were driven together by arterial pulse transformation—was postulated. Pulsatile movements were observed in the aqueduct, foramen of Monro, basal cisterns, and spinal subarachnoid space, especially at the cervical level. DuBoulay et al. [11] concluded that pulsation of the CSF was due to pulsation in the vascular system.

The transmission of the arterial pulse pressure wave to the brain has already occurred by the time ventricular systole has ended, about 280 msec after the R wave. Diastole follows immediately and results in a prompt drop-off in pulse pressure within the carotid arteries and brain [12].

A comparison of the DTDA and STDA images shows that the foramen of Monro expands in systole as compared with diastole. The CSF moved to the aqueduct, which received more CSF in systole and was wider compared with diastole. Similar observations have been made by Citrin et al. [12]. More pronounced pulsatile flow in systole as compared with diastole was observed in the fourth ventricle, foramen of Magendie, cisterna magna, and cervical level of the spinal subarachnoid space. There was no significant change in the basal cisterns.

High-velocity flow produced greater phase shifts and thus higher signal intensity because of incomplete rephasing proportional to velocity. In the absence of flow, signal intensity loss was registered since stationary nuclei were all brought back into phase by the rephasing pulse after initial dephasing. These changes in signal intensity, depending on the presence of CSF flow at systolic and diastolic times, made it possible to demonstrate obstructive lesions in the CSF pathway. This not only increased the understanding of the pathogenesis of these lesions but also influenced the management strategy.

It was not possible in this present series to obtain absolute proof of the function of a "thalamic pump," either in patients or in normal volunteers, but there was a clear dependence of CSF pulsation on the systolic and diastolic times of the cardiac cycle. Flow in the lateral ventricles was not observed in any case, but this could only be finally resolved with improved sensitivity of the present imaging sequence. The resolution of the problem of directionality of flow requires improved techniques that can demonstrate flow in all directions with satisfactory image quality. Despite these present limitations, MR-GILD offers potential for the investigation of disorders involving the CSF circulation.

ACKNOWLEDGMENT

We thank F. Marguth, who showed interest in this work.

REFERENCES

1. Singer IR, Crooks LE. Nuclear magnetic resonance blood flow measurement in human brain. *Science* **1983**;221:654–656
2. Axel L. Blood flow effects in magnetic resonance imaging. *AJR* **1984**;143:1157–1166
3. Wedeen VJ, Meuli RA, Edelmann RR, et al. Projective imaging of pulsatile flow with magnetic resonance. *Science* **1985**; 230:946–948
4. Meuli RA, Wedeen VJ, Geller SC, et al. MR gated subtraction angiography: evaluation of lower extremities. *Radiology* **1986**;159:411–418
5. Sherman JL, Citrin CM. Magnetic resonance demonstration of normal CSF flow. *AJNR* **1986**;7:3–6
6. Sherman JL, Citrin CM, Gangarosa RE, Bowen BJ. The MR appearance of CSF flow in patients with ventriculomegaly. *AJNR* **1986**;7:1025–1031
7. Ridgway JP, Smith MM. A technique for velocity imaging using MRI. *Br J Radiol* **1986**;59:603–607
8. Francois J. Heredity of craniofacial dysostoses. *Mod Probl Ophthalmol* **1975**;14:5–48
9. O'Connell JEA. The vascular factor in intracranial pressure and the maintenance of the cerebrospinal fluid circulation. *Brain* **1943**;73:165–172
10. Bering EA. Choroid plexus and arterial pulsation of the choroid plexuses as a cerebrospinal fluid pump. *Arch Neurol Psychiatry* **1955**;73:165–172
11. DuBoulay G, O'Connell J, Currie J, Bostic T, Verity P. Further investigations on pulsatile movements in the cerebrospinal fluid pathways. *Acta Radiol* **1972**;13:496–523
12. Citrin CM, Sherman JL, Gangarosa RE, Scanlon D. Physiology of the CSF flow-void sign: modification by cardiac gating. *AJNR* **1986**;7:1021–1024